

Influence of complex phonon spectra on intersubband optical gain

Mikhail V. Kisin and Vera B. Gorfinkel

Department of Electrical Engineering, State University of New York at Stony Brook, Stony Brook, New York 11794-2350

Michael A. Stroscio

US Army Research Office, PO Box 12211, Research Triangle Park, North Carolina 27709-2211

Gregory Belenky^{a)} and Serge Luryi

Department of Electrical Engineering, State University of New York at Stony Brook, Stony Brook, New York 11794-2350

(Received 23 April 1997; accepted for publication 4 June 1997)

Electron-phonon scattering rates and intersubband optical gain spectra were calculated, including the optical phonon confinement effect in AlGaAs/GaAs/AlGaAs quantum well heterostructures. Comparison of the calculated gain spectra with those calculated using the bulk phonon approximation shows that details of the phonon spectrum have a strong influence on the intersubband optical gain. © 1997 American Institute of Physics. [S0021-8979(97)07517-8]

I. INTRODUCTION

The intersubband optical gain in a quantum well is one of the key parameters determining the performance of a quantum cascade laser (QCL). Positive intersubband optical gain can be achieved at any level of carrier concentration, provided there is a population inversion at the wavelength of interest. The population inversion in a QCL is defined mainly by the ratio of the intersubband scattering rate and the lower subband depopulation rate in the active quantum well.¹ Successful device design, therefore, requires a correct calculation of both the intersubband transition rate and the lower subband depopulation rate. In the present article, we show that taking into account the realistic heterostructure phonon spectrum is essential for accurate determination of the intersubband scattering rate in QCL. Laser optical gain spectra calculated using the realistic phonon spectrum are significantly different from those obtained in the bulk phonon approximation. The intersubband optical gain spectra were obtained for an AlGaAs/GaAs/AlGaAs quantum well with electron subbands calculated including the nonparabolicity of electron energy spectrum. The optical phonon spectrum of the heterostructure was described in terms of confined, interface, and half-space barrier phonons by using the dielectric continuum model.²

II. THE MODEL

Electron spectrum: Spectral characteristics of the QCL are strongly influenced by the phase relaxation processes for

the electron states participating in the intersubband radiative transition.^{3,4} As a simplest model of the QCL unit cell, we consider a symmetric double heterostructure AlGaAs/GaAs/AlGaAs with a GaAs layer of width a such that the structure supports at least two subbands in the resulting quantum well; see Fig. 1. Since the inclusion of the subband nonparabolicity is essential for correct description of QCL operation,³ we calculate the electron energy spectrum on the basis of the four-band Kane model. Both the complex boundary conditions for multicomponent wave functions⁵ and the finite values of energy band offsets at heterointerfaces are taken into account to obtain an accurate description of high energy electronic states, especially in the second subband. The electron wave functions for confined electron states in the n th subband are taken in the form

$$\Psi_{\mathbf{K}}^{(n)}(\mathbf{R}) = \frac{1}{\sqrt{Sa}} e^{i\mathbf{K}\mathbf{r}} \psi_{\mathbf{K}}^{(n)}(z); \quad \mathbf{R} = (\mathbf{r}, z); \quad \mathbf{r} = (x, y). \quad (1)$$

In this article, we concentrate on the electron energy states in the conduction band only and therefore we can simplify the description of the electron wave functions by reducing the four-component Kane wave function envelopes $\psi_{\mathbf{K}}^{(n)}$ to scalar functions.

1st subband:

$$\psi_1(z) = \sqrt{2} C_1 \begin{cases} \cos(k_1 z); & |z| < \frac{a}{2}; \\ \cos\left(\frac{k_1 a}{2}\right) e^{-\lambda_1(|z| - a/2)}; & |z| > \frac{a}{2}; \end{cases} \quad k_1 \tan \frac{k_1 a}{2} = \lambda_1 \frac{E_{w1}}{E_{b1}}, \quad (2a)$$

^{a)}Electronic mail: postmaster@sbee.sunysb.edu

2nd subband:

$$\psi_2(z) = \sqrt{2}C_2 \begin{cases} \sin(k_2 z); & |z| < \frac{a}{2}; \\ \text{sign}(z) \sin \frac{k_2 a}{2} e^{-\lambda_2(|z| - a/2)}; & |z| > \frac{a}{2}; \end{cases}$$

Here the energy origin in each layer, well (w) or barrier (b), is taken at the top of the valence band in the corresponding material; for example,

$$\begin{aligned} E_{w1,2} &= E_{g_w} + E_{1,2}(K) \\ &= E_{g_w} + E_{1,2}(0) + \varepsilon_{1,2}(K), \end{aligned} \quad (3)$$

where $E_b = E_w + \Delta_V$.

The dispersion relation of the Kane model gives expressions for k and λ , which describe the electron energy spectrum

$$\left(\frac{2m_c}{\hbar^2 E_g} E(E - E_g) - K^2 \right)_{w,b} = \begin{cases} k^2 & (w) \\ -\lambda^2 & (b). \end{cases} \quad (4)$$

An exemplary subband calculation for an $\text{Al}_x\text{Ga}_{1-x}\text{As}/\text{GaAs}/\text{Al}_x\text{Ga}_{1-x}\text{As}$ double heterostructure with Al fraction $x=0.3$ are shown in Fig. 1. Energy band offsets in this case are $\Delta_c=300$ meV and $\Delta_V=150$ meV. The width of the GaAs layer was chosen to be $a=6$ nm in order to support two electron subbands. These subbands are shown in Fig. 1 with solid lines. To facilitate comparison, dashed lines illustrate the subband structure for the well width $a=10$ nm.

Phonon spectrum: The phonon spectrum of a heterostructure consists of three types of longitudinal-optical (LO) phonon modes which have been shown to be important for electron energy relaxation processes: confined modes (c),

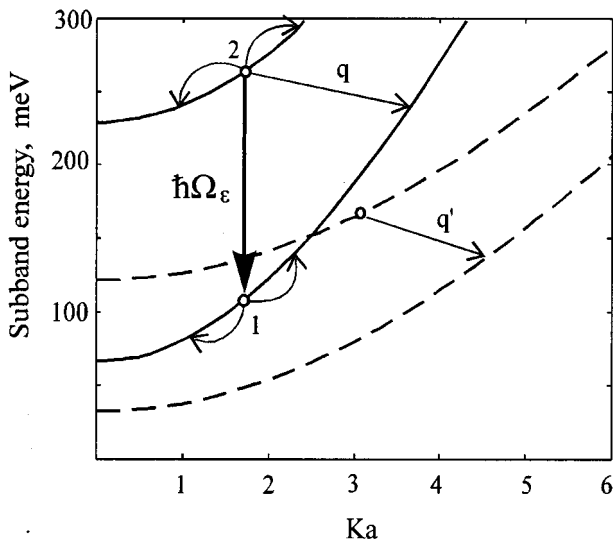


FIG. 1. Intersubband and intrasubband transitions in the active quantum well of QCL. The quantum well parameters used: $E_g(\text{GaAs})=1.4$ eV, $\Delta_c=0.3$ eV, $\Delta_V=0.15$ eV, $m_c(\text{GaAs})=0.067$. Subbands shown for quantum well width: $a=6$ nm—solid lines; $a=10$ nm—dashed lines.

$$k_2 \cot \frac{k_2 a}{2} = -\lambda_2 \frac{E_{w2}}{E_{b2}}. \quad (2b)$$

symmetrical or antisymmetrical interface modes (is, ia), and half-space barrier (b) modes in the cladding layer.² The interaction hamiltonians for each type of phonons are

$$e\Phi_{\mathbf{q}}^{(m)}(\mathbf{R}) = \left(\frac{e^2 \hbar \omega_m(q)}{2 \varepsilon_0 q S} \right)^{1/2} e^{i\mathbf{q}\mathbf{R}} \phi_{\mathbf{q}}^{(m)}(z) \mu_m(q). \quad (5)$$

Functions $\mu_m(q)$ contain the effective dielectric constants for different phonon modes and can be easily found from expressions given in Ref. 2. Here the phonon mode potential envelopes $\phi_{\mathbf{q}}^{(m)}$ are taken in the usual form

$$\begin{aligned} \phi_q^{(is)}(z) &= \begin{cases} \cosh(qz)/\cosh \frac{qa}{2}; & |z| < \frac{a}{2} \\ \exp[-q(|z| - a/2)]; & |z| > \frac{a}{2} \end{cases} \\ \phi_q^{(ia)}(z) &= \begin{cases} \sinh(qz)/\sinh \frac{qa}{2}; & |z| < \frac{a}{2} \\ \text{sign}(z) \exp\left(-q\left(|z| - \frac{a}{2}\right)\right); & |z| > \frac{a}{2} \end{cases} \\ \phi_q^{(c1)} &= \cos \frac{\pi z}{a}; \quad \phi_q^{(c2)} = \sin \frac{2\pi z}{a}; \quad \dots \quad |z| < \frac{a}{2}, \\ \phi_{q,q_z}^{(b)} &= (z) \sin\left[q_z\left(|z| - \frac{a}{2}\right)\right]; \quad |z| > \frac{a}{2}. \end{aligned} \quad (6)$$

Electron-phonon interaction: We use these results to calculate the corresponding partial scattering rates $W_{n,n',m}^{(\pm)}$ for electron transitions from the n subband to n' subband due to absorption (+) or emission (-) of m -type phonons

$$\begin{aligned} W_{n,n',m}^{(\pm)}(\mathbf{K}) &= \frac{S}{(2\pi)^2} \int d^2\mathbf{q} \frac{2\pi}{\hbar} |M_{n,n',m}|^2 \\ &\quad \times \delta[E_n(\mathbf{K}) \pm \hbar \omega_m(\pm \mathbf{q}) - E_{n'}(\mathbf{K} + \mathbf{q})] \\ &\quad \times \left\{ \begin{array}{l} N_{\mathbf{q}}^{(m)} \\ N_{-\mathbf{q}}^{(m)} + 1 \end{array} \right\}. \end{aligned} \quad (7)$$

In this analysis, we ignore the effect of phonon heating and assume the phonon distribution function, $N_{\mathbf{q}}^{(m)}$, to be the equilibrium Bose-Einstein distribution function. Additionally, we consider the electron initial state to be occupied and the final state to be empty. The matrix element in (7) can be represented as,

$$\begin{aligned} M_{n,n',m}(q) &= \int d^3\mathbf{R} \Psi_{\mathbf{K}+\mathbf{q}}^{(n')\pm} e\Phi_{\mathbf{q}}^{(m)} \Psi_{\mathbf{K}}^{(n)} \\ &= \left(\frac{e^2 \hbar \omega_m(q)}{2 \varepsilon_0 q S} \right)^{1/2} \mu_m(q) F_{n,n',m}(q). \end{aligned} \quad (8)$$

It contains the interaction form-factor $F_{n,n',m}$ which is independent of material parameters and describes the overlap of the smooth electron envelope functions $\psi_{\mathbf{K}}^{(n)}$ and the phonon macroscopic potential envelope $\phi_{\mathbf{q}}^{(m)}$:

$$F_{n,n',m}(q) = \frac{1}{a} \int dz \psi_{\mathbf{K}+\mathbf{q}}^{(n')\dagger}(z) \psi_{\mathbf{K}}^{(n)}(z) \phi_{\mathbf{q}}^{(m)}(z). \quad (9)$$

A K dependence of the form factors is introduced as a result of the nonparabolicity of the electron energy spectrum but is practically negligible in the case of GaAs-based heterostructures. Below, we present the form factors for different scattering processes. For confined and interface phonons:

$$F_{n,n,cl} = C_n^2 \left\{ \frac{\sin(l\pi/2)}{l\pi/2} - (-1)^n \left[\frac{\sin(ak_n + l\pi/2)}{ak_n + l\pi/2} + \frac{\sin(ak_n - l\pi/2)}{ak_n - l\pi/2} \right] \right\}, \quad (10)$$

$$F_{2,1,cl} = C_2 C_1 \left\{ - \frac{\sin 0.5[l\pi + a(k_2 + k_1)]}{l\pi + a(k_2 + k_1)} + \frac{\sin 0.5[l\pi - a(k_2 + k_1)]}{l\pi - a(k_2 + k_1)} - \frac{\sin 0.5[l\pi + a(k_2 - k_1)]}{l\pi + a(k_2 - k_1)} + \frac{\sin 0.5[l\pi - a(k_2 - k_1)]}{l\pi - a(k_2 - k_1)} \right\}, \quad (11)$$

$$F_{n,n,is} = \frac{2C_n^2}{a} \left\{ \frac{1 - (-1)^n \cos ak_n}{q + 2\lambda_n} + \frac{1}{q} \left[\tanh \frac{aq}{2} - \frac{(-1)^n q^2}{q^2 + 4k_n^2} \left(\tanh \frac{aq}{2} \cos ak_n + \frac{2k_n}{q} \sin ak_n \right) \right] \right\}, \quad (12)$$

and

$$F_{2,1,ia} = \frac{2C_2 C_1}{a} \left\{ \frac{2}{\lambda_1 + \lambda_2 + q} \sin \frac{ak_2}{2} \cos \frac{ak_1}{2} + \frac{1}{q \sinh(aq/2)} \left[\frac{1}{1 + (k_1 + k_2)^2/q^2} \left(\cosh \frac{aq}{2} \sin \frac{a(k_1 + k_2)}{2} - \frac{k_1 + k_2}{q} \sinh \frac{aq}{2} \cos \frac{a(k_1 + k_2)}{2} \right) + \frac{1}{1 + (k_2 - k_1)^2/q^2} \left(\cosh \frac{aq}{2} \sin \frac{a(k_2 - k_1)}{2} - \frac{k_2 - k_1}{q} \sinh \frac{aq}{2} \cos \frac{a(k_2 - k_1)}{2} \right) \right] \right\}. \quad (13)$$

In the case of a single symmetric quantum well, the number of phonon modes participating in the scattering processes is essentially reduced by the parity selection rules.⁶

$$W_{n \rightarrow n} = W_{n,n}^{(is-)} + W_{n,n}^{(is+)} + W_{n,n}^{(cl)} + W_{n,n}^{(b)}, \quad (14)$$

$$W_{2 \rightarrow 1} = W_{2,1}^{(ia-)} + W_{2,1}^{(ia+)} + W_{2,1}^{(cl)} + W_{2,1}^{(b)}.$$

Here only even (cos-like) confined modes ($l=1,3,\dots$) can participate in intrasubband scattering processes and only odd (sin-like) confined modes ($l=2,4,\dots$) participate in intersubband processes. We remark that selection rules (14) hold strictly under the assumption of scalar electron wave functions and would not be valid in the case of a strong nonparabolicity. For two possible interface modes of each parity, we use the same notations ($i\pm$) and dispersion relations as in Ref. 2 assuming that $\omega_{is+} > \omega_{is-}$ and $\omega_{ia+} > \omega_{ia-}$. We also use a one-mode approximation for interface phonons, assuming the interaction of electrons with GaAs-like split alloy mode to be weak⁷ and, therefore, neglecting this mode in interface phonon spectra. Alloy splitting of phonon frequencies is indeed important for the barrier phonon modes. We can take into account modifying the interaction strength for different barrier modes as in Ref. 7

$$\left(\frac{1}{\kappa_b(\infty)} - \frac{1}{\kappa_b(0)} \right) \frac{\hbar \omega_b e^2}{2\varepsilon_0} \rightarrow \frac{\hbar e^2}{\varepsilon_0} \left(\frac{\partial \kappa_b(\omega)}{\partial \omega} \right)^{-1}_{\omega_b = \omega_{LC}, \omega_{LD}}. \quad (15)$$

Here the dielectric function in the barrier alloy material is represented phenomenologically by

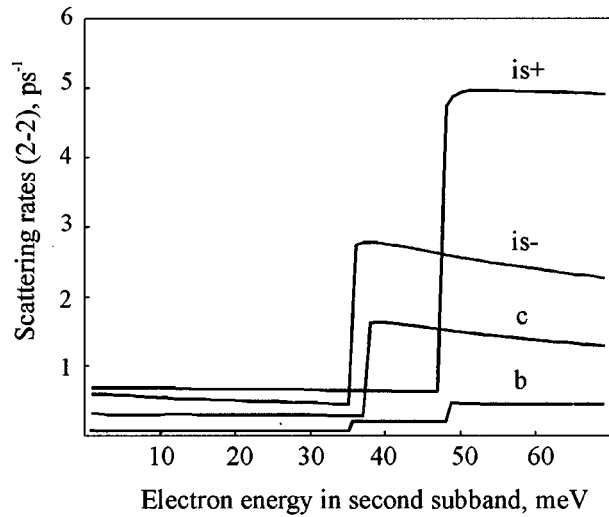
$$\kappa_b(\omega) = \kappa_b(\infty) \frac{(\omega^2 - \omega_{LC}^2)(\omega^2 - \omega_{LD}^2)}{(\omega^2 - \omega_{TC}^2)(\omega^2 - \omega_{TD}^2)}, \quad (16)$$

so that the barrier region is characterized by two alloy split LO-phonon modes: an AlAs-like mode with frequency ω_{LC} and a GaAs-like mode with frequency ω_{LD} . Because of the constant value of split barrier mode frequencies, it is possible to carry out the summation over all transverse phonon wave vectors q_z and to define the effective matrix element for barrier phonon scattering:

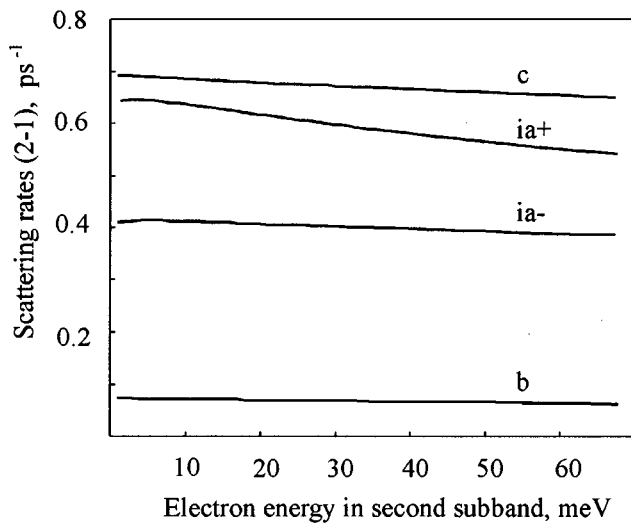
$$|M_{\text{eff}}^{(b)}|^2 = \frac{L_z}{2\pi} \left(\frac{\hbar \omega_b e^2}{2\varepsilon_0 S q} \right)^2 \int_{-\infty}^{\infty} dq_z [\mu_b(q_z) F_b(q_z)]^2. \quad (17)$$

As a result, the form factor for this scattering process can be represented as

$$F_{n,n'}^{(b)}(q_z) = \frac{1}{a} \frac{2q_z C_n C_{n'}}{(\lambda_n + \lambda_{n'})^2 + q_z^2} \left\{ \left[1 + \left(\frac{E_{wn} \lambda_n}{E_{bn} k_n} \right)^2 \right] \times \left[1 + \left(\frac{E_{wn'} \lambda_{n'}}{E_{bn'} k_{n'}} \right)^2 \right] \right\}^{-1/2}. \quad (18)$$



(a)

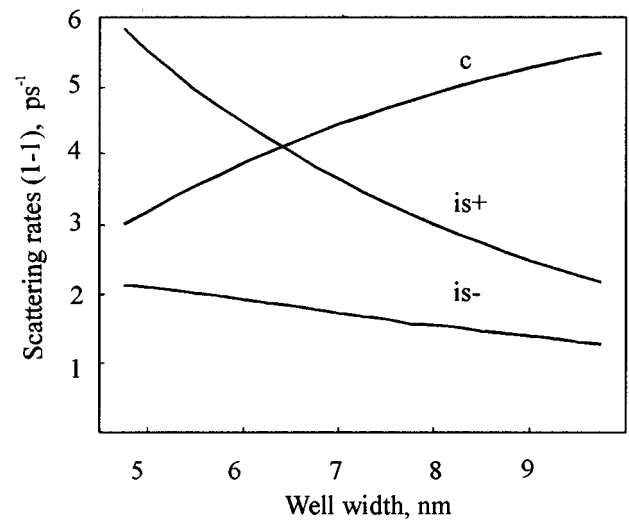


(b)

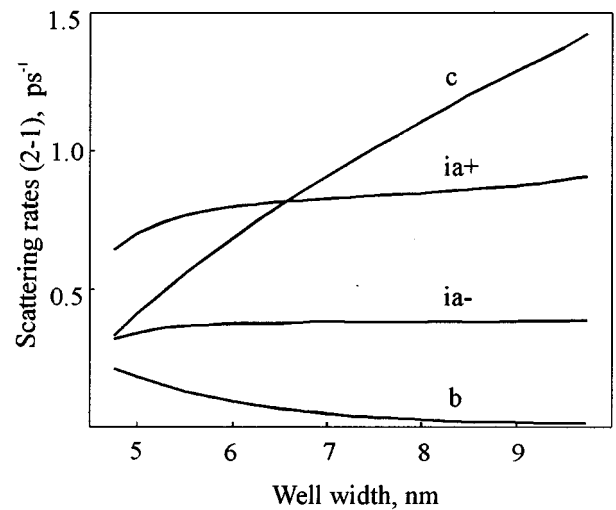
FIG. 2. Intrasubband $2 \rightarrow 2$ scattering rates for different phonon modes as a function of electron energy for $\text{Al}_x\text{Ga}_{1-x}\text{As}/\text{GaAs}/\text{Al}_x\text{Ga}_{1-x}\text{As}$ heterostructure at room temperature. The heterostructure parameters are: $x=0.4$, $\Delta_c=300$ meV, $\Delta_v=200$ meV, $a=6$ nm. (a) Intrasubband $2 \rightarrow 2$ scattering rates. Here c —confined phonon mode, $is \pm$ —two types of the symmetrical interface modes participating in intrasubband scattering, and b —half-space barrier phonon mode in the cladding layer. (b) Intersubband $2 \rightarrow 1$ scattering rates. Here: c —confined phonon mode, $ia \pm$ —two types of the antisymmetrical interface modes participating in intersubband scattering, and b —half-space barrier phonon mode in the cladding layer.

III. SCATTERING RATE CALCULATIONS

Figure 2 shows the energy dependence of scattering rates for different phonon modes in the case of intrasubband $2 \rightarrow 2$ scattering processes at room temperature. The relevant physical parameters used in this calculation are listed in Table I. The interface modes dominate in electron-phonon scattering for such a thin quantum well.^{2,6,8} In a heterostruc-



(a)



(b)

FIG. 3. Dependence of scattering rates for different phonon modes on well width. (a) Intrasubband $1 \rightarrow 1$ processes. Here: c —confined phonon mode, $is \pm$ —two types of the symmetrical interface modes participating in intrasubband scattering. For electron states in the first subband, barrier mode scattering is negligible and is not shown. Initial electron energy in first subband is $\varepsilon_1=60$ meV. (b) Intersubband $2 \rightarrow 1$ processes. Here: c —confined phonon mode, $ia \pm$ —two types of the antisymmetrical interface modes participating in intersubband scattering, and b —half-space barrier phonon mode in the cladding layer. Initial electron energy in second subband is $\varepsilon_2=10$ meV.

ture with a low enough energy barrier in the conduction band, it is possible for the electron wave function to penetrate deeper into the barrier region.⁹ This concerns especially the high energy electron states in the second subband of a quantum well. As a result, barrier phonon scattering becomes significant for intrasubband $2 \rightarrow 2$ scattering events; see curve b in Fig. 2(a). The two steps on the curve for barrier-type scattering are accounted for by the alloy splitting

of barrier phonon modes.⁷ The data used for split phonon modes in $\text{Al}_x\text{Ga}_{1-x}\text{As}$ were taken from Ref. 10 and are represented in Table I.

The well width is a critical parameter in determining the electron-phonon scattering because of its strong influence on the overlap of phonon and electron envelope functions. Substantial redistribution occurs between scattering rates corresponding to the different phonon modes when the well width is changed. Figures 3(a) and 3(b) illustrate the dependence on the well width for scattering rates corresponding to intrasubband $1 \rightarrow 1$ [Fig. 3(a)] and intersubband $2 \rightarrow 1$ [Fig. 3(b)] transitions. In the first case, the electron kinetic energy was taken to be $\varepsilon_1 = 60$ meV. In the second case, the electron energy was fixed at the level $\varepsilon_2 = 10$ meV from the bottom of the second subband. It is interesting to note the anomalous behavior of intersubband interface phonon scattering rates as a function of well width a [Fig. 3(b)]. As a matter of fact, the decreasing overlap of the electron and interface phonon envelopes results in the interaction form-factors $F_{n,n'}^{(is,ia)}(q_a)$ which are also quite rapidly decreasing functions of the well width a . For intrasubband transitions, this leads to the decreasing character of the corresponding scattering rates, see

Fig. 3(a), curves $is \pm$. From another point of view, the decrease in subband energy separation $q' < q$ participating in the intersubband transitions in a quantum well with $a' > a$; see, for example, Fig. 1. When the subband separation becomes comparable with the energy of the phonon, the contribution of the scattering events with small momentum transfer becomes more valuable, especially for interface-phonon-assisted processes, for which even the resonant condition can appear.¹¹

Quasibulk approximation: It is a common view that for purposes of intrawell electron relaxation analysis, it is sufficient to approximate the real phonon spectrum of the heterostructure by the effective bulk phonon spectrum.¹²⁻¹⁴ As we shall see below, this approximation is inadequate in the case of the QCL because of the high sensitivity of the optical gain to the details of electron-phonon scattering. For the purpose of comparison, let us derive the corresponding formula for the confined electron-bulk phonon (B) scattering rates in order to evaluate the influence of model used on the calculated optical gain spectra. Otherwise, we use the same approximations that we employed in deriving Eqs. (7) and (8); we find

$$W_{n,n',B}^{(\pm)} = \frac{1}{(2\pi)^3} \int dq_z \int d^2\mathbf{q} \frac{2\pi}{\hbar} \frac{e^2 \hbar \omega_B}{2\varepsilon_0(q^2 + q_z^2)} \left(\frac{1}{\kappa(\infty)} - \frac{1}{\kappa(0)} \right) \left[\int dz \psi_{\mathbf{K}+\mathbf{q}}^{(n')\pm}(z) \psi_{\mathbf{K}}^{(n)}(z) e^{iq_z z} \right]^2 \delta[E_n(\mathbf{K}) \pm \hbar \omega_B - E_{n'}(\mathbf{K}+\mathbf{q})] \left\{ \frac{N_q^{(B)}}{N_q^{(B)} + 1} \right\} = \left(\frac{m_c e^2 \hbar \omega_B}{2\varepsilon_0 \kappa_{\text{eff}}} \right) \left(\frac{E_n(K) \pm \hbar \omega_B}{E_g} - 1 \right) \left\{ \frac{N_q^{(m)}}{N_q^{(m)} + 1} \right\} \frac{1}{2\pi} \int_{-\infty}^{\infty} \frac{dq_z F_{i,j}^2}{\sqrt{(q_z^2 + q_1^2)(q_z^2 + q_2^2)}}. \quad (19)$$

Here q_1 and q_2 are the limiting values for the in-plane phonon wave vector \mathbf{q} . The form factors for the particular processes are

$$F_{n,n}^{(B)} = \frac{C_n^2}{a} \left\{ 2(1 - (-1)^n \cos ak_n) \times \frac{2\lambda_n \cos(0.5aq_z) + q_z \sin(0.5aq_z)}{4\lambda_n^2 + q_z^2} + 2 \frac{\sin(0.5aq_z)}{q_z} - (-1)^n \left[\frac{\sin a(0.5q_z + k_2)}{q_z + 2k_2} + \frac{\sin a(0.5q_z - k_2)}{q_z - 2k_2} \right] \right\}, \quad (20)$$

$$F_{2,1}^{(B)} = \frac{C_2 C_1}{a} \left\{ 4 \sin \frac{ak_2}{2} \cos \frac{ak_1}{2} \times \frac{(\lambda_1 + \lambda_2) \sin(0.5aq_z) + q_z \cos(0.5aq_z)}{(\lambda_1 + \lambda_2)^2 + q_z^2} - \frac{\sin 0.5a(q_z + k_2 + k_1)}{q_z + k_2 + k_1} + \frac{\sin 0.5a(q_z - k_2 + k_1)}{q_z - k_2 + k_1} - \frac{\sin 0.5a(q_z + k_2 - k_1)}{q_z + k_2 - k_1} + \frac{\sin 0.5a(q_z - k_2 - k_1)}{q_z - k_2 - k_1} \right\}. \quad (21)$$

It was argued in Ref. 15, that the sum rule for electron-phonon interaction in a quantum well causes the exact value of the total scattering rate to lie between the calculated rates for the interaction with well (GaAs) and barrier (AlGaAs) bulk phonons. However, this is true only if we are not concerned with the phonon energy dependence of scattering rate, because the sum rule is restricted to matrix elements. This situation is clearly seen from Figs. 4(a) and 4(b) where dashed and dashed-dotted curves correspond to the limiting scattering rates with bulk phonons of GaAs (dashed curve) and AlGaAs (dashed-dotted curve). The curve corresponding to AlGaAs phonons exhibits a two-step behavior as a result of the alloy splitting of phonon modes in the alloy material. Scattering rates calculated in the quasibulk approximation include the scattering events for the same initial and final confined electron states but with only bulk phonon modes involved. The total scattering rates for the real phonon spectrum of the heterostructure (solid curve) obey the above sum rule in the high energy region, where scattering rates are practically dispersionless. The situation is quite different for electron kinetic energies near $\varepsilon \approx \hbar \omega_{ph}$, that is in the electron energy range of 35–50 meV, where the strong energy dependence of scattering rates results from the threshold behavior of the phonon emission processes. The sum rule fails in this energy range even qualitatively. This fact should have

a strong influence on the optical gain calculations because the energies near $\varepsilon \approx \hbar \omega_{ph}$ are typical for hot or injected electrons in the heterostructure subbands.

IV. CALCULATIONS OF INTERSUBBAND OPTICAL GAIN

We calculate the optical gain spectrum $g(\Omega)$ in accordance with the theory presented in Refs. 3 and 4,

$$g(\Omega) = \frac{4\pi n_2 e^2 |z_{12}|^2 \Omega}{\hbar a c \sqrt{\kappa_\infty} k T_e} \int_0^\infty d\varepsilon \tau_\varepsilon(\Omega) e^{-\varepsilon/kT_e} \left(1 - \frac{f_1}{f_2} \right). \quad (22)$$

Here $\tau_\varepsilon(\Omega)$ is the line shape function

$$\tau_\varepsilon(\Omega) = \frac{W(\varepsilon)}{[\Omega - \Omega_\varepsilon]^2 + [W(\varepsilon)]^2}, \quad (23)$$

and emitted phonon energy corresponds to a particular ‘‘vertical’’ transition

$$\hbar \Omega_\varepsilon = E_2(K) - E_1(K) = \hbar \Omega_0 + \varepsilon_2(K) - \varepsilon_1(K).$$

The vertical transition can be described by only one independent variable, $\varepsilon \equiv \varepsilon_2$, since for a given K (neglecting the photon momentum) the energy ε_2 determines ε_1 and vice versa; see Fig. 1. The damping term $W(\varepsilon)$ results primarily from the optical-phonon assisted scattering events that break the phase coherence of electron states participating in the radiative transition, that is,

$$W(\varepsilon) = \sum_{ijm(\pm)} W_{ijm}^{(\pm)}(\mathbf{K}). \quad (24)$$

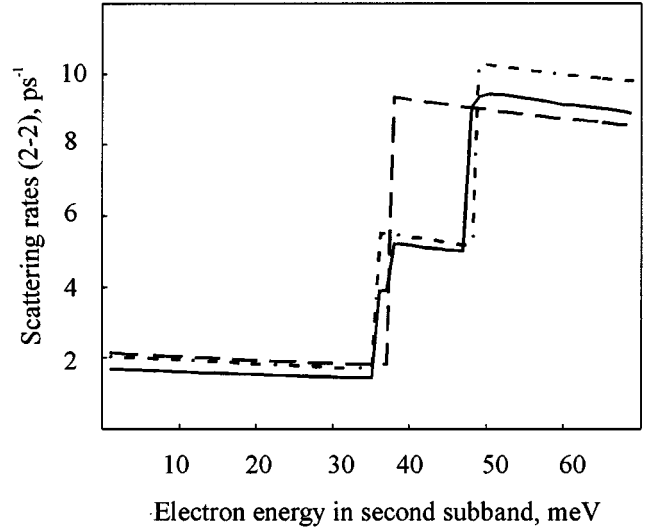
The electron concentration in the second subband was taken to be $n_2 = 10^{11} \text{ cm}^{-2}$. At this moderate level of injection, we can use Boltzmann statistics, because even for electron temperatures as low as $T_e = 100 \text{ K}$, we have $n_2/N_c \ll 1$, where $N_c = m^* k T_e / \pi \hbar^2$ is the effective density of states in a 2D subband. The ratio of the distribution functions in (22) can be represented in a particularly simple form if we assume that the subbands themselves are parabolic—but with different effective masses m_1 and m_2 . In this case, we have $\varepsilon_1 = \varepsilon m_2 / m_1$ and

$$\frac{f_1}{f_2} = \frac{n_1 m_2}{n_2 m_1} \exp \left[\frac{\varepsilon}{k T_e} \left(1 - \frac{m_2}{m_1} \right) \right]. \quad (25)$$

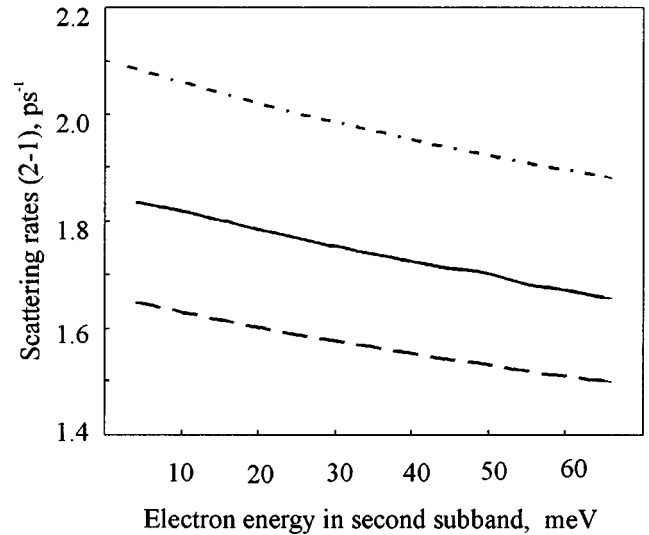
TABLE I. Heterostructure parameters used in calculations.

Al _x Ga _{1-x} As/GaAs/Al _x Ga _{1-x} As heterostructure parameters			
a	6 nm	x	0.4
m_c (GaAs)	$0.067 m_0$	Δ_c	300 meV
$E_g \omega$ (GaAs)	1.4 eV	Δ_v	200 meV
Lattice parameters			
Well material (GaAs)		Barrier material (Al _x Ga _{1-x} As)	
$\hbar \omega_L$	36.2 meV	$\hbar \omega_{LC}$	46.8 meV
		$\hbar \omega_{LD}$	34.3 meV
$\hbar \alpha_T$	33.3 meV	$\hbar \omega_{TC}$	44.6 meV
		$\hbar \omega_{TD}$	32.9 meV
K_∞	10.9	K_∞	10.1

Room temperature gain spectra calculations are presented in Figs. 5 and 6. Figure 5 illustrates an attempt to approximate the realistic phonon spectrum of the heterostructure by bulk phonons of GaAs (dashed curves) or GaAlAs (dashed-dotted curves) as has been described above. The solid curves represent the results of calculations when the complex phonon spectrum of the heterostructure are taken into account. The gain spectra are calculated for different values of the characteristic time of lower subband depopulation, $\tau_{\text{out}}^{(1)}$: 0.4 and 0.6 ps [Fig. 5(a)]; and 0.55 ps

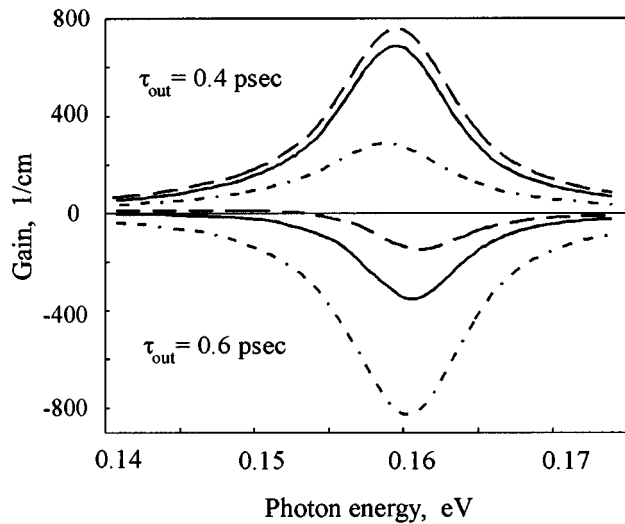


(a)

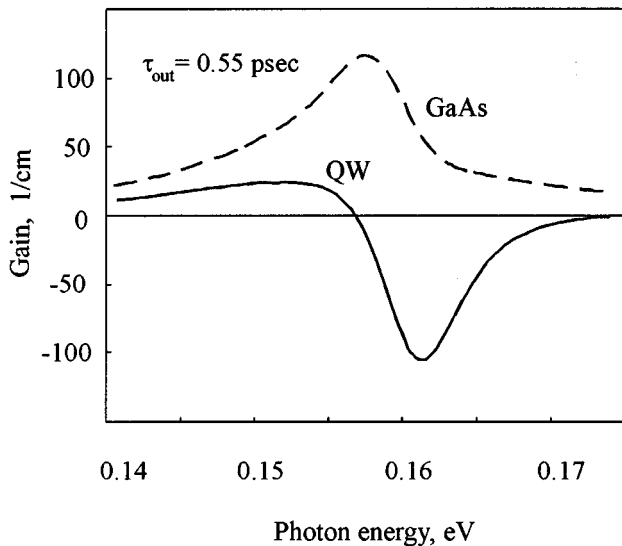


(b)

FIG. 4. Comparison of the total scattering rate calculated for real phonon spectrum and scattering rates calculated in quasibulk approximation for intrasubband 2 → 2 (a) and intersubband 2 → 1 (b) transitions. The curves in the figures are marked: **dashed line**—approximation of real phonon spectrum with bulk GaAs phonons; **dashed-dotted line**—approximation of real phonon spectrum with bulk GaAlAs phonons, **solid line**—real quantum well phonon spectrum was taken into account.



(a)



(b)

FIG. 5. Optical gain calculated in different phonon spectrum models and for different values of lower subband depopulation time, $\tau_{\text{out}}^{(1)}$: 0.4 and 0.6 (a); 0.55 ps (b). The curves in the figures are marked: **dashed line**—approximation of real phonon spectrum with bulk GaAs phonons; **dashed-dotted line**—approximation of real phonon spectrum with bulk GaAlAs phonons, **solid line**—real quantum well (QW) phonon spectrum was taken into account.

[Fig. 5(b)]. The time $\tau_{\text{out}}^{(1)}$ describes phenomenologically the electron escape process from the lower subband and is to be determined by the prevalent escape mechanism, e.g., by the optical¹⁶ or tunneling evacuation.¹ High sensitivity of the optical gain to the value of this parameter is a consequence of its strong dependence on the difference between the distribution functions in Eq. (22) and, as a result, on the ratio between the subband populations n_1 and n_2 in Eq. (25). The last ratio is directly related to the ratio between the charac-

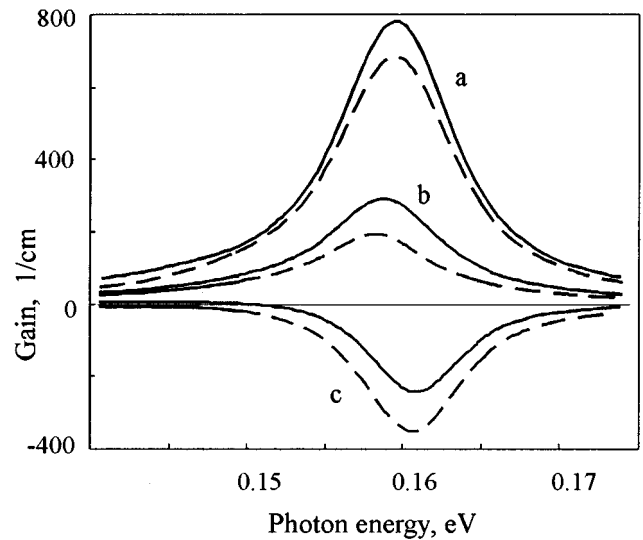


FIG. 6. Influence of the phonon spectrum fine structure on the intersubband optical gain spectra: **dashed line**—all phonon modes are taken into account, **solid line**—without barrier phonon modes in the $2 \rightarrow 1$ intersubband scattering processes. First subband depopulation time $\tau_{\text{out}}^{(1)}$ used in the calculations: (a) 0.4; (b) 0.5; and (c) 0.6 ps.

teristic times of subband depopulation,⁴ $\tau_{21} = 1/W_{21}$ and $\tau_{\text{out}}^{(1)}$, because of the particle flow conservation condition in steady state $n_2/\tau_{21} = n_1/\tau_{\text{out}}^{(1)}$. As a result, it also implies high sensitivity of the optical gain to the intersubband scattering rate value W_{21} . The last quantity may differ according to the phonon spectrum model used, see Fig. 4(b), and this difference, even when small, is capable of causing significant changes in the optical characteristics of a QCL heterostructure, as we see in Fig. 5. This influence is especially important in the regime when $\tau_{21} \approx \tau_{\text{out}}^{(1)}$, which seems to be the prevalent regime in reported QCL heterostructures. The results calculated for $\tau_{\text{out}}^{(1)} = 0.55$ ps are shown in Fig. 5(b). For the heterostructure considered in our exemplary calculations, we obtain the room temperature value of the characteristic intersubband scattering time to be $\tau_{21} = 0.56$ ps. This value characterizes the scattering rate for an electron with kinetic energy $\varepsilon_2 \approx kT_e$. The gain spectrum in this critical situation is crucially determined by the small difference between occupation probabilities of electron states in the first and the second subbands. Figure 5(b) shows that owing to the non-parabolicity of electron energy subbands the occupation probability of the state ε_2 in the upper subband can be higher than that of the state ε_1 in the lower subband.⁴ Figure 5(b) also shows the result of gain spectrum calculation with the phonon spectrum of the heterostructure approximated by bulk phonons of GaAs (dashed line). We conclude that an attempt to use the quasibulk approximation of phonon spectra in the QCL heterostructure dramatically changes the calculated optical characteristics and, therefore, is not suitable for device design purpose.

Figure 6 gives another example of the sensitivity of calculated optical gain spectra to details of the phonon spectrum. For illustrative purposes, we use the example of barrier phonon scattering which becomes sensible for the $2 \rightarrow 1$ in-

tersubband transitions in the case of sufficiently thin GaAs layers; see Fig. 3(b). Barrier phonon modes are usually ignored in device analysis¹⁷ because they are comparatively small. However, even when small, the enhancement of the intersubband scattering rate due to barrier phonon modes can change the optical gain of a QCL heterostructure, as we see in Fig. 6. The calculations were performed for three different values of the depopulation time of lower subband $\tau_{\text{out}}^{(1)}$: 0.4 (a), 0.5 (b), and 0.6 ps (c). In each case, the dashed curve represents the gain spectrum calculated taking into account all the phonon modes in the double heterostructure and the solid curve represents exemplary results neglecting barrier modes scattering. In these two situations, the characteristic intersubband scattering rates for an electron with kinetic energy $\varepsilon_2 \approx kT_e$ do not differ significantly and were found to be $W_{21} = 1.77, 1.70 \text{ ps}^{-1}$, correspondingly. Nevertheless, it is seen quite clearly that under the condition $\tau_{21} \approx \tau_{\text{out}}^{(1)}$ the optical gain spectra appear to be very sensitive even to such fine details of the phonon spectrum.

V. CONCLUSION

Electron–phonon scattering rates and intersubband optical gain spectra were considered, including the optical phonon confinement effect in the description of electron–phonon interaction in AlGaAs/GaAs/AlGaAs quantum well heterostructures. Comparison of the gain spectra obtained for the case of phonon confinement with the gain spectra calculated using the bulk phonon approximation shows a significant influence of the phonon spectrum fine structure on the intersubband optical gain. This demonstrates the necessity of in-

cluding the optical phonon confinement effects in the quantitative design of quantum wells for the active region of quantum cascade lasers.

ACKNOWLEDGMENTS

The authors would like to thank Dr. B. L. Gelmont for his critical review of this work and helpful discussions. This work is supported by the U.S. Army Research Office.

- ¹J. Faist, F. Capasso, C. Sirtori, D. L. Sivco, A. L. Hutchinson, and A. Y. Cho, *Appl. Phys. Lett.* **66**, 538 (1995).
- ²N. Mori and T. Ando, *Phys. Rev. B* **40**, 6175 (1989).
- ³B. Gelmont, V. Gorfinkel, and S. Luryi, *Appl. Phys. Lett.* **68**, 2171 (1996).
- ⁴V. Gorfinkel, S. Luryi, and B. Gelmont, *IEEE J. Quantum Electron.* **32**, 1995 (1996).
- ⁵M. V. Kisin, *Semiconductors* **30**, 928 (1996); **28**, 1143 (1994); **27**, 274 (1993).
- ⁶J. K. Jain and S. Das Sarma, *Phys. Rev. Lett.* **62**, 2305 (1989); S. Das Sarma, V. B. Campos, M. A. Stroscio, and K. W. Kim, *Semicond. Sci. Technol.* **7**, B60 (1992).
- ⁷K. W. Kim and M. A. Stroscio, *J. Appl. Phys.* **68**, 6289 (1990).
- ⁸M. A. Stroscio, G. J. Iafrate, K. W. Kim, M. A. Littlejohn, H. Goronkin, and G. N. Maracas, *Appl. Phys. Lett.* **59**, 1093 (1991).
- ⁹Y. T-Dai, Y. F. Chen, and I. Lo, *Phys. Rev. B* **55**, 5235 (1997).
- ¹⁰*Landolt–Bornstein Tables*, edited by O. Madelung (Springer, Berlin, 1987), Group III, Vol. 22a, pp. 136–139.
- ¹¹M. A. Stroscio, *J. Appl. Phys.* **80**, 6854 (1996).
- ¹²S. Das Sarma and B. A. Mason, *Ann. Phys.* **163**, 78 (1985).
- ¹³R. Ferreira and G. Bastard, *Phys. Rev. B* **40**, 1074 (1989).
- ¹⁴J. H. Smet, C. G. Fonstad, and Q. Hu, *J. Appl. Phys.* **79**, 9305 (1996).
- ¹⁵H. Rucker, E. Molinari, and P. Lugli, *Phys. Rev. B* **45**, 6747 (1992).
- ¹⁶A. Kastalsky, *IEEE J. Quantum Electron.* **29**, 1112 (1993).
- ¹⁷J. Wang, J. P. Leburton, F. H. Julien, and A. Sa'ar, *Superlattices Microstruct.* **20**, 245 (1996).